Wind and Structures, Vol. 9, No. 2 (2006) 159-178
DOI: http://dx.doi.org/10.12989/was.2006.9.2.159

Identification of 18 flutter derivatives by covariance driven stochastic subspace method

Shambhu Sharan Mishra†

Department of Civil Engineering, NERIST, Nirjuli, Arunachal Pradesh 791109, India

Krishen Kumar‡ and Prem Krishna†‡

Department of Civil Engineering, Indian Institute of Technology, Roorkee 247667, India

(Received March 14, 2005, Accepted March 7, 2006)

Abstract. For the slender and flexible cable supported bridges, identification of all the flutter derivatives for the vertical, lateral and torsional motions is essential for its stability investigation. In all, eighteen flutter derivatives may have to be considered, the identification of which using a three degree-of-freedom elastic suspension system has been a challenging task. In this paper, a system identification technique, known as covariance-driven stochastic subspace identification (COV-SSI) technique, has been utilized to extract the flutter derivatives for a typical bridge deck. This method identifies the stochastic state-space model from the covariances of the output-only (stochastic) data. All the eighteen flutter derivatives have been simultaneously extracted from the output response data obtained from wind tunnel test on a 3-DOF elastically suspended bridge deck section-model. Simplicity in model suspension and measurements of only output responses are additional motivating factors for adopting COV-SSI technique. The identified discrete values of flutter derivatives have been approximated by rational functions.

Keywords: flutter derivative; wind tunnel test; stochastic subspace identification; rational function approximation.

1. Introduction

Long span cable supported bridges are susceptible to the wind-induced actions and may become critical to flutter. Flutter is an aeroelastic, self-excited phenomenon resulting in growing amplitude of oscillation of the bridge structure due to the interaction of aerodynamic, inertial and elastic forces. The analysis for critical flutter wind speed is based on flutter derivatives (Scanlan and Tomko 1971, Scanlan 1978) which are extracted from the wind tunnel tests on a geometrically scaled section-model of the bridge deck. The experimental extraction of the flutter derivatives is possible but not without difficulties. Among the different investigators Sarkar, *et al*. (1994) used

† Professor, Corresponding Author, E-mail: chadyaneha_sunny@yahoo.co.in; ssm@agni.nerist.ac.in
‡ Professor, E-mail: iswe@iitr.ernet.in
†‡ Professor, E-mail: pkrcpfce@iitr.ernet.in

Modified Ibrahim Time Domain (MITD) method and extracted eight flutter derivatives out of the full set of 18 flutter derivatives which are currently in use for expressing the general self-excited forces. Brownjohn and Jakobsen (2001) used Covariance Block-Hankel Matrix (CBHM) method while Gu, *et al.* (2000) and Zhu, *et al.* (2002) used Unifying Least Squares (ULS) technique to identify eight flutter derivatives. Qin and Gu (2004) applied Stochastic Subspace Identification technique to identify six flutter derivatives.

Identification of 18 flutter derivatives for bridge deck-sections has also been tried by some investigators. Singh, *et al.* (1995) extended the MITD method for identifying all the eighteen flutter derivatives but lacked clear trends of H_6^*, A_5^*, A_6^*, P_3^*, P_5^* and P_6^* due to large scatter of identified values. Chen, *et al.* (2002) used general Least Squares theory and compared the flutter derivatives with those obtained by computational fluid dynamics but at the higher wind speeds most of the flutter derivatives except H_1^*, H_2^*, H_3^*, A_1^*, A_2^*, and A_3^* did not compare well. Chowdhury and Sarkar (2003, 2004) used Iterative Least Squares (ILS) technique to determine eighteen flutter derivatives from the estimated state matrix after generating the velocity and acceleration data numerically by finite differencing of available displacement time-history. Though the trends of the identified flutter derivatives were clear, the lengths of records selected were not sufficiently long. Also, the generation of velocity and acceleration by finite differencing of displacements, especially at the ends, lacked convergence.

The above system identification techniques require versatile three degree of freedom suspension system which is difficult to realize in practice. Also, the length of records obtained from the free vibration testing are very short especially at higher wind speeds and thus identification of flutter derivatives is not accurate and representative of the actual wind environment. The above mentioned problems can be circumvented by using the stochastic method of system identification in which the wind itself excites the section- model which is freely suspended to oscillate in the wind tunnel. The turbulence in the wind as input to the motion may be assumed as the unmeasureable stochastic quantity. This assumption further reduces the instrumentation in the measurement of data. The lengths of records can be taken long enough even at higher wind speeds for better accuracy in system identification.

A technique of system identification known as Stochastic Subspace Identification (SSI) method has gained popularity over the recent years which has been well developed and applied by Overschee and Moor (1993), Peeters and Roeck (1999) and Peters (2000) for system identifications. The method requires only the measurement of output response data for extraction of the system parameters and has proved to be very appropriate for civil engineering structures.

In this paper, a variant of the SSI method known as the Covariance-Driven Stochastic Subspace Identification (COV-SSI) method has been applied as a system identification technique to extract all the eighteen flutter derivatives from the wind tunnel test output data for a section-model of a long span cable-stayed bridge-deck. The motivation for identification of all the eighteen flutter derivatives by the COV-SSI technique came from Qin and Gu (2004) who applied the method to extract six flutter derivatives, namely H_1^*, H_2^*, H_3^* A_1^*, A_2^* and A_3^*.

The heart of the COV-SSI technique is the eigen-system realization algorithm (ERA) developed by Juang and Pappa (1985) for the modal parameters of a system. This method identifies the stochastic state-space model from the covariances of the output-only (stochastic) data and has been proved as robust against nonstationary inputs (e.g. a white noise sequence with time varying covariances).

The method has been described in the coming sections in the following sequence. First, the

mathematical model of the system in discrete time form and then the theory identifying the modal parameters from the covariances of output measurements is presented. Next, the formulations for determining the physical stiffness and damping coefficients from the corresponding modal parameters are shown. Finally, the formulations for the flutter derivatives followed by a very concise description of approximation of flutter derivatives by rational function approximation are presented. A description about the experimental setup, acquisition and processing of displacement output data has also been presented.

2. Modeling of the system

2.1. Discrete time system representation

The discrete time state-space description of a linear time invariant (LTI) vibrating system, considering a fixed sampling interval, Δt, is expressed at any time, $t_k = k\ \Delta t$, $k \in N$, as:

$$\boldsymbol{x}_{k+1} = \boldsymbol{A}\boldsymbol{x}_k + \boldsymbol{B}\boldsymbol{u}_k \tag{1}$$

Eq. (1) is known as the process equation. The discrete time output (measurement) equation is expressed as:

$$\boldsymbol{y}_k = \boldsymbol{C}\boldsymbol{x}_k + \boldsymbol{D}\boldsymbol{u}_k \tag{2}$$

where $\boldsymbol{x}_k = \boldsymbol{x}(\boldsymbol{k}\ \Delta \boldsymbol{t}) = \{\boldsymbol{q}_k^T \dot{\boldsymbol{q}}_k^T\}^T$ is the discrete-time state vector containing the discretely sampled displacements $\boldsymbol{q}_k$ and velocities $\dot{\boldsymbol{q}}_k$; $\boldsymbol{u}_k$ and $\boldsymbol{y}_k$ are the discretely sampled input and output respectively; $\boldsymbol{A}$ is the discrete-time state matrix; $\boldsymbol{B}$ is the discrete input matrix; $\boldsymbol{C}$ is the discrete output locator matrix; $\boldsymbol{D}$ is the direct transmission matrix. They are related with their continuous time counterparts and can be found elsewhere such as in Juang (1994).

2.2. Stochastic process and measurement equations

In real world of experiments, some imperfections in the measurements and in the process describing the system are inherent. Therefore, stochastic noise terms are also included in the process and measurement equations. By the stochastic system we consider that the input is unmeasureable and is embedded in the white noise. Therefore, in this formulation the distinction between the input terms and the noise terms is dropped and only the stochastic noise terms are retained to incorporate implicitly the input, $\boldsymbol{u}_k$ in them. Then, the following combined discrete time state-space model is obtained:

$$\begin{aligned} \boldsymbol{x}_{k+1} &= \boldsymbol{A}\boldsymbol{x}_k + \boldsymbol{w}_k \\ \boldsymbol{y}_k &= \boldsymbol{C}\boldsymbol{x}_k + \boldsymbol{v}_k \end{aligned} \tag{3}$$

where $\boldsymbol{w}_k$ is the process noise due to disturbances and modeling inaccuracies; $\boldsymbol{v}_k$ is the measurement noise due to output sensor inaccuracies.

3. Stochastic system identification

Following assumptions are imposed on the stochastic discrete model: (i) model is stationary; (ii)

$\boldsymbol{x}_k$, $\boldsymbol{w}_k$ and $\boldsymbol{v}_k$ are independent with zero mean; and (iii) $\boldsymbol{w}_k$ and $\boldsymbol{v}_k$ are unmeasureable vector quantities. With these assumptions the stochastic system matrices are determined on the analogy of deterministic system matrices (Ho and Kalman 1966). Knowing the mathematical model, Eq. (3), that represents the system the output covariance sequences, $\boldsymbol{R}_i$, can be estimated from the output measurement data. If this sequence is decomposed, the stochastic realization of the matrices $\boldsymbol{A}$ and $\boldsymbol{C}$ can be obtained (Akaike 1974).

3.1. Covariance estimate

The output covariances, $\boldsymbol{R}_i$ can now be expressed assuming ergodicity of process as:

$$\boldsymbol{R}_i = E(\boldsymbol{y}_{k+i}\boldsymbol{y}_k^T) = \lim_{N\to\infty} \frac{1}{N}\sum_{k=0}^{N-1} \boldsymbol{y}_{k+i}\,\boldsymbol{y}_k^T \tag{4}$$

where $i > 0$ is an arbitrary time lag. $\boldsymbol{R}_i$, after dropping the limit for only finite number N of data, can be estimated as:

$$\boldsymbol{R}_i \approx \boldsymbol{R}_i = \frac{1}{N}\sum_{k=0}^{N-1} \boldsymbol{y}_{k+i}\,\boldsymbol{y}_k^T \tag{5}$$

3.2. Realisation of discrete-time state matrix

The output covariances, Eq. (5), are collected in a block Toeplitz matrix $\boldsymbol{T}_{1|i}$ as:

$$\boldsymbol{T}_{1|i} = \begin{bmatrix} \boldsymbol{R}_i & \boldsymbol{R}_{i-1} & \cdots & \boldsymbol{R}_1 \\ \boldsymbol{R}_{i+1} & \boldsymbol{R}_i & \cdots & \boldsymbol{R}_2 \\ \cdots & \cdots & \cdots & \cdots \\ \boldsymbol{R}_{2i-1} & \boldsymbol{R}_{2i-2} & \cdots & \boldsymbol{R}_i \end{bmatrix} \tag{6}$$

If the system is observable and controllable, the rank of the Toeplitz matrix equals $n = 2n_1$ where n_1 is the degree of freedom of the system. Then the factorization in terms of observability and controllability matrices can be written as:

$$\boldsymbol{T}_{1|i} = \boldsymbol{O}_i \Gamma_i \tag{7}$$

where the definitions of observability matrix, $\boldsymbol{O}_i$, and controllability matrix, Γ_i, can be found in any book on control theory or modern system identification e.g., Ljung (1987).

The singular value decomposition (SVD) of the block Toeplitz matrix $\boldsymbol{T}_{1|i}$ gives:

$$\boldsymbol{T}_{1|i} = \boldsymbol{U}\boldsymbol{S}\boldsymbol{V}^T \approx \boldsymbol{U}_1\boldsymbol{S}_1\boldsymbol{V}_1^T = \boldsymbol{U}_1\boldsymbol{S}_1^{1/2}\boldsymbol{S}_1^{1/2}\boldsymbol{V}_1^T \tag{8}$$

where $\boldsymbol{U}$, $\boldsymbol{S}$ and $\boldsymbol{V}$ are orthonormal matrices. Matrix $\boldsymbol{S}$ is a diagonal matrix containing positive singular values in descending order. The number of nonzero singular values indicates the rank of the Toeplitz matrix. The reduced diagonal matrix $\boldsymbol{S}_1$ is obtained by omitting the zero singular values from the matrix $\boldsymbol{S}$. Matrices $\boldsymbol{U}_1$ and $\boldsymbol{V}_1$ are obtained by omitting the corresponding columns from

the matrices $\boldsymbol{U}$ and $\boldsymbol{V}$ respectively.

From Eq. (7) and last equality of Eq. (8), observability and controllability matrices can be given as:

$$\begin{aligned} \boldsymbol{O}_i &= \boldsymbol{U}_1 \boldsymbol{S}_1^{1/2} \\ \boldsymbol{\Gamma}_i &= \boldsymbol{S}_1^{1/2} \boldsymbol{V}_1^T \end{aligned} \tag{9}$$

Now realizations of the system matrices are almost achieved. Matrix $\boldsymbol{A}$ is realized by using factorization of a shifted Toeplitz matrix $\boldsymbol{T}_{2|i+1}$ as shown in Zeiger and McEwen (1974). The shifted block Toeplitz matrix, $\boldsymbol{T}_{2|i+1}$ has similar structure as of $\boldsymbol{T}_{1|i}$ but it consists of covariances, $\boldsymbol{R}_k$ from lag 2 to $2i$. The state transition matrix, $\boldsymbol{A}$ is given as:

$$\boldsymbol{A} = \boldsymbol{O}_i^+ \boldsymbol{T}_{2|i+1} \boldsymbol{\Gamma}_i^+ = \boldsymbol{S}_1^{-1/2} \boldsymbol{U}_1^T \boldsymbol{T}_{2|i+1} \boldsymbol{V}_1 \boldsymbol{S}_1^{-1/2} \tag{10}$$

where (+) stands for Moore-Penrose pseudo inverse of a matrix.

The output locator matrix $\boldsymbol{C}$ is taken as the first l rows of observability matrix $\boldsymbol{O}_i$, where l is the number of outputs. Here, $l = 3$. $\boldsymbol{A}$ and $\boldsymbol{C}$ are sufficient to compute the modal parameters.

3.3. Modal frequency and damping

After knowing the discrete time state matrix, $\boldsymbol{A}$ $(n \times n)$, its discrete time eigenvalue matrix, Λ and modal matrix, $\boldsymbol{\Psi}$ can be determined. The observed mode shape matrix, $\boldsymbol{\Phi} = \boldsymbol{C}\boldsymbol{\Psi}$. $\boldsymbol{\Phi}$ contains n vectors of system modes as complex conjugate pairs. Λ is a diagonal matrix containing n complex eigenvalues, λ_{Di}, corresponding to the i th mode, given as:

$$\lambda_{Di}, \lambda_{Di,}^* = -\zeta_i \omega_i \pm j\omega_i \sqrt{1-\zeta_i^2} \tag{11}$$

where (*) denotes the complex conjugate and $j = \sqrt{-1}$. The continuous time eigenvalues, λ_{Ci}, are then obtained by as:

$$\lambda_{Ci} = \frac{\ln(\lambda_{Di})}{\Delta t} = a_i \pm j b_i \tag{12}$$

The undamped frequency of the system is given as:

$$\omega_i = \sqrt{a_i^2 + b_i^2} \tag{13}$$

and damping ratio ζ is given as

$$\zeta_i = \frac{a_i}{\omega_i} \tag{14}$$

Frequencies defined by Eq. (13) in general differ from the corresponding natural frequencies of the original system. The size of the matrix $\boldsymbol{A}$ depends on the number of nonsingular values selected from the $\boldsymbol{S}$ matrix in Eq. (8). An economical model order may be selected by selecting the rows and columns of $\boldsymbol{S}$ matrix where large gap in two consecutive nonzero values occur. The singular value where large gap occurs determines the model order or the size of matrix $\boldsymbol{A}$. The order of matrix $\boldsymbol{A}$ so obtained is generally greater than the actual order of the matrix $\boldsymbol{A}_c$. This is equivalent to saying that model so selected represents a system that has more degrees of freedom than of the actual

system. A reduction in modal degrees of freedom using Guyan (1965) reduction technique may then be applied to obtain the system parameters corresponding to the actual model order.

3.4. Physical stiffness and damping coefficient

Let $\boldsymbol{M}$, $\boldsymbol{C}_1$ and $\boldsymbol{K}$ be respectively, the system's physical mass, damping coefficient and stiffness matrices of size $n_1 \times n_1$. Matrix, $\boldsymbol{C}_1$, in the present study, has been determined by assuming a proportional damping case. The modal damping coefficient matrix $\overline{\boldsymbol{C}}$ is given as:

$$\overline{\boldsymbol{C}} = \boldsymbol{\Phi}^T \boldsymbol{C}_1 \boldsymbol{\Phi} = diag[2\zeta_i \omega_i \overline{M}_i] \tag{15}$$

where ζ_i, ω_i, $\overline{M}_i$ are the ith modal damping ratio, frequency and mass respectively. The modal mass matrix is given as:

$$\overline{\boldsymbol{M}} = \boldsymbol{\Phi}^T \boldsymbol{M} \boldsymbol{\Phi} \tag{16}$$

Then the physical damping matrix $\boldsymbol{C}_1$ is given as (Craig 1981):

$$\boldsymbol{C}_1 = (\boldsymbol{M}\boldsymbol{\Phi}\overline{\boldsymbol{M}}^{-1})\overline{\boldsymbol{C}}(\overline{\boldsymbol{M}}^{-1}\boldsymbol{\Phi}^T\boldsymbol{M}) \tag{17}$$

and the physical stiffness matrix $\boldsymbol{K}$ is obtained from the eigenvalue problem as:

$$\boldsymbol{K}\boldsymbol{\Phi} = \boldsymbol{M}\boldsymbol{\Phi}\boldsymbol{\Lambda} \tag{18}$$

Therefore,

$$\boldsymbol{K} = \boldsymbol{M}\boldsymbol{\Phi}\boldsymbol{\Lambda}\boldsymbol{\Phi}^{-1} \tag{19}$$

4. Formulation for flutter derivatives

Let the bridge deck section-model of width B is has a vertical mass, m_h lateral mass, m_p and mass moment of inertia, I_α per unit length along the vertical (h), lateral (p) and torsional (α) degrees of freedom respectively. ζ_h, ζ_p, and ζ_α, are the mechanical or inherent damping ratios and ω_h, ω_p, and ω_α, are the natural frequencies corresponding to the three degrees of freedom respectively. These values are obtained from free vibration records of the section model under no-wind condition. Assuming that $\boldsymbol{C}^{mech}$ and $\boldsymbol{K}^{mech}$ are the matrices of mechanical damping coefficient and stiffness under no-wind condition, the equation of motion for the section model subjected to self-excited aeroelastic forces may be written as:

$$\ddot{\boldsymbol{y}} + \boldsymbol{M}^{-1}\boldsymbol{C}\dot{\boldsymbol{y}} + \boldsymbol{M}^{-1}\boldsymbol{K}\boldsymbol{y} = \boldsymbol{M}^{-1}\boldsymbol{F}_{se} \tag{20}$$

where,

$$\boldsymbol{y} = \{h \quad \alpha \quad p\}^T, \quad \boldsymbol{M} = \begin{bmatrix} m_h & 0 & 0 \\ 0 & I_\alpha & 0 \\ 0 & 0 & m_p \end{bmatrix}$$

$$\boldsymbol{M}^{-1}\boldsymbol{C} = \begin{bmatrix} 2\zeta_h\omega_h & 0 & 0 \\ 0 & 2\zeta_\alpha\omega_\alpha & 0 \\ 0 & 0 & 2\zeta_p\omega_p \end{bmatrix} = \boldsymbol{C}^{mech}, \quad \boldsymbol{M}^{-1}\boldsymbol{K} = \begin{bmatrix} \omega_h^2 & 0 & 0 \\ 0 & \omega_\alpha^2 & 0 \\ 0 & 0 & \omega_p^2 \end{bmatrix} = \boldsymbol{K}^{mech}$$

The aeroelastic force vector $\boldsymbol{F}_{se}$ which a model is subjected to in air stream of velocity U and density ρ is given as:

$$\boldsymbol{F}_{se} = \begin{Bmatrix} L_{se} \\ M_{se} \\ D_{se} \end{Bmatrix} = \begin{bmatrix} 0.5\rho U^2 B & 0 & 0 \\ 0 & 0.5\rho U^2 B^2 & 0 \\ 0 & 0 & 0.5\rho U^2 B \end{bmatrix}$$

$$\begin{bmatrix} KH_1^*/U & KH_2{}^*B/U & KH_5^*/U & K^2H_4^*/B & K^2H_3^* & K^2H_6^*/B \\ KA_1^*/U & KA_2{}^*B/U & KA_5^*/U & K^2A_4^*/B & K^2A_3^* & K^2A_6^*/B \\ KP_5^*/U & KP_2{}^*B/U & KP_1^*/U & K^2P_6^*/B & K^2P_3^* & K^2H_4^*/B \end{bmatrix} \begin{Bmatrix} \dot{h} \\ \dot{\alpha} \\ \dot{p} \\ h \\ \alpha \\ p \end{Bmatrix} \tag{21}$$

where, L_{se}, D_{se} and M_{se} are the aeroelastic (self-excited) forces induced in the model in the lift, drag and pitching moment directions; $K = B\omega/U$ is the reduced frequency; ω is the circular frequency of oscillation; H_i^*, A_i^* and P_i^* $(i = 1, 2, \ldots, 6)$ are the flutter derivatives.

Substituting Eq. (21) in Eq. (20) and bringing all terms to the left side, the aeroelastically modified equations of motion are obtained:

$$\ddot{\boldsymbol{y}} + \boldsymbol{C}^{eff}\dot{\boldsymbol{y}} + \boldsymbol{K}^{eff}\boldsymbol{y} = 0 \tag{22}$$

where, $\boldsymbol{C}^{eff}$ and $\boldsymbol{K}^{eff}$ are the aeroelastically modified effective damping and stiffness matrices respectively. Then Eq. (22) can be written in state-space form as:

$$\dot{\boldsymbol{X}} = \boldsymbol{A}_c\boldsymbol{X} \tag{23}$$

where, $\boldsymbol{X} = \begin{bmatrix} \boldsymbol{y} \\ \dot{\boldsymbol{y}} \end{bmatrix}$, $\boldsymbol{A}_c = \begin{bmatrix} 0 & \boldsymbol{I} \\ -\boldsymbol{K}^{eff} & -\boldsymbol{C}^{eff} \end{bmatrix}$

The state matrix $\boldsymbol{A}_c$ is a $2n_1 \times 2n_1$ matrix $(n_1 = 3)$ and $\boldsymbol{I}$ is an $n_1 \times n_1$ identity matrix. The submatrices $\boldsymbol{C}^{eff}$ and $\boldsymbol{K}^{eff}$ $(n_1 \times n_1)$ are obtained by using Eqs. (17) and (19) after realization of modal damping ratio and frequency from Eqs. (13) and (14) respectively. Then, the flutter derivatives are obtained from the following formulations:

$$H_1^* = -\frac{2m_h}{\rho B^2\omega}(C_{11}^{eff} - C_{11}^{mech}) \tag{24a}$$

$$H_2^* = -\frac{2m_h}{\rho B^3 \omega}(C_{12}^{eff} - C_{12}^{mech}) \tag{24b}$$

$$H_3^* = -\frac{2m_h}{\rho B^3 \omega^2}(K_{12}^{eff} - K_{12}^{mech}) \tag{24c}$$

$$H_4^* = -\frac{2m_h}{\rho B^2 \omega^2}(K_{11}^{eff} - K_{11}^{mech}) \tag{24d}$$

$$H_5^* = -\frac{2m_h}{\rho B^2 \omega}(C_{13}^{eff} - C_{13}^{mech}) \tag{24e}$$

$$H_6^* = -\frac{2m_h}{\rho B^2 \omega^2}(K_{13}^{eff} - K_{13}^{mech}) \tag{24f}$$

$$A_1^* = -\frac{2I_\alpha}{\rho B^3 \omega}(C_{21}^{eff} - C_{21}^{mech}) \tag{24g}$$

$$A_2^* = -\frac{2I_\alpha}{\rho B^4 \omega}(C_{22}^{eff} - C_{22}^{mech}) \tag{24h}$$

$$A_3^* = -\frac{2I_\alpha}{\rho B^4 \omega^2}(K_{22}^{eff} - K_{22}^{mech}) \tag{24i}$$

$$A_4^* = -\frac{2I_\alpha}{\rho B^3 \omega^2}(K_{21}^{eff} - K_{21}^{mech}) \tag{24j}$$

$$A_5^* = -\frac{2I_\alpha}{\rho B^3 \omega}(C_{23}^{eff} - C_{23}^{mech}) \tag{24k}$$

$$A_6^* = -\frac{2I_\alpha}{\rho B^3 \omega^2}(K_{23}^{eff} - K_{23}^{mech}) \tag{24l}$$

$$P_1^* = -\frac{2m_p}{\rho B^2 \omega}(C_{33}^{eff} - C_{33}^{mech}) \tag{24m}$$

$$P_2^* = -\frac{2m_p}{\rho B^2 \omega}(C_{32}^{eff} - C_{32}^{mech}) \tag{24n}$$

$$P_3^* = -\frac{2m_p}{\rho B^3 \omega^2}(K_{32}^{eff} - K_{32}^{mech}) \tag{24o}$$

$$P_4^* = -\frac{2m_p}{\rho B^2 \omega^2}(K_{33}^{eff} - K_{33}^{mech}) \tag{24p}$$

$$P_5^* = -\frac{2m_p}{\rho B^2 \omega}(C_{31}^{eff} - C_{31}^{mech}) \tag{24q}$$

$$P_6^* = -\frac{2m_p}{\rho B^2 \omega^2}(K_{31}^{eff} - K_{31}^{mech}) \tag{24r}$$

5. Rational function approximation of flutter derivatives

Flutter derivatives are the functions of the reduced frequencies, K, and they are known only at discrete frequencies. To obtain flutter derivatives (hence frequency dependent aeroelastic forces) as a continuous function of reduced frequencies, rational function approximation of flutter derivatives is used. The rational function approximation technique was originally presented by Roger (1977) and commonly used by Bucher and Lin (1988), Boonyapinyo, *et al.* (1999), Chen, *et al.* (2000a, b), Chen and Kareem (2002) for representation of self-excited forces, is given by:

$$\boldsymbol{Q}_{se}(r) = \boldsymbol{a}_1^* + \boldsymbol{a}_2^* r + \boldsymbol{a}_3^* r^2 + \sum_{l=1}^{l=m} r\frac{\boldsymbol{a}_{l+3}^*}{r + b_l} \tag{25}$$

where the rational function coefficients $\boldsymbol{a}_1^*$, $\boldsymbol{a}_2^*$, $\boldsymbol{a}_3^*$ and $\boldsymbol{a}_{l+3}^*$ are frequency independent (3×3) matrices. $\boldsymbol{a}_1^*$, $\boldsymbol{a}_2^*$, $\boldsymbol{a}_3^*$, $\boldsymbol{a}_{l+3}^*$ and b_l are obtained from the known values of flutter derivatives by curve fitting and applying nonlinear least squares technique, and $l = 1, 2, \ldots, m$. The first term of the right hand side rational approximation represents the noncirculatory static-aerodynamic term whereas the second term represents the aerodynamic damping. The third term represents the aerodynamic mass and the rational term (last term) accounts for the nonlinearity and unsteadiness in the flow and represents a lag from the velocity of oscillation. The positive value of b approximates a time delay in the motion of the model. The value of m may be taken from 2 to 4 depending on the convergence and the number of lag terms (rational terms). 'r' is a nondimensional Laplace variable given as $r = iK = sB/U$, where $s = i\omega$ and $i = \sqrt{-1}$. Forces in Laplace domain can now be obtained as follows:

Expressing Eq. (21) in terms of non-dimensional Laplace variable r gives:

$$\begin{Bmatrix} \overline{L_{se}} \\ \overline{D_{se}} \\ \overline{M_{se}} \end{Bmatrix} = \frac{1}{2}\rho U^2 \begin{bmatrix} B & 0 & 0 \\ 0 & B & 0 \\ 0 & 0 & B^2 \end{bmatrix} \begin{bmatrix} K^2(iH_1^* + H_4^*) & K^2(iH_5^* + H_6^*) & K^2(iH_2^* + H_3^*) \\ K^2(iP_5^* + P_6^*) & K^2(iP_1^* + P_4^*) & K^2(iP_2^* + P_3^*) \\ K^2(iA_1^* + A_4^*) & K^2(iA_5^* + A_6^*) & K^2(iA_2^* + A_3^*) \end{bmatrix} \begin{Bmatrix} \left(\frac{\overline{h}}{B}\right) \\ \left(\frac{\overline{p}}{B}\right) \\ \overline{\alpha} \end{Bmatrix} \tag{26}$$

with Eqs. (25) and (26), flutter derivatives can be expressed in terms of rational function as:

$$\begin{bmatrix} K^2(iH_1^* + H_4^*) & K^2(iH_5^* + H_6^*) & K^2(iH_2^* + H_3^*) \\ K^2(iP_5^* + P_6^*) & K^2(iP_1^* + P_4^*) & K^2(iP_2^* + P_3^*) \\ K^2(iA_1^* + A_4^*) & K^2(iA_5^* + A_6^*) & K^2(iA_2^* + A_3^*) \end{bmatrix} = \boldsymbol{a}_1^* + \boldsymbol{a}_2^* r + \boldsymbol{a}_3^* r^2 + \sum_{l=1}^{l=m} r\frac{\boldsymbol{a}_{l+3}^*}{r + b_l} \tag{27}$$

Eq. (27) finally, on equating the imaginary and real terms, flutter derivatives can be obtained in terms of rational function coefficients and reduced frequency, K. For example

$$H_1^* = \frac{1}{K}\left[a_2^* + \sum_{l=1}^{m} \frac{a_{l+3}^*}{b_l^2 + K^2} b_l\right] \tag{28a}$$

$$H_4^* = \left[\frac{a_1^*}{K^2} - a_3^* + \sum_{l=1}^{m} \frac{a_{l+3}^*}{b_l^2 + K^2}\right] \tag{28b}$$

The parameters $\boldsymbol{a}_i^*$ ($i = 1,\ldots, m+3$) have been determined by the nonlinear least-squares fit using Levenberg-Marquardt method (Bevington 1969, Press, *et al.* 1992). The values of parameter b_l ($l = 1,\ldots, m$) have been kept fixed as $= \{0.5, 2.0, 5.0, 7\}$ for $m = 4$ to ensure convergence of the function and reduce the number of aerodynamic states which are generally used for further aeroelastic analysis.

6. Experimental setup and signal processing technique

6.1. Wind tunnel characteristics

The wind tunnel tests were performed in the boundary layer wind tunnel at the Indian Institute of Technology, Roorkee (India). The tunnel has a working section of 2.0 m width and 2.1 m height. Wind speed could be generated continuously from 0.5 m/s to 18 m/s while maintaining a constant speed at any level in the range with the help of a dynodrive system. Wind speeds were measured manually by using a properly calibrated manometer as well as a Hot-Wire Anemometer. The extraction of flutter derivatives has been carried out under smooth flow. Therefore, the turbulence in the flow was made to a minimum (less than 2% of U) level to ensure a smooth wind for the test.

6.2. Description of the section-model

The bridge deck section-model (Fig. 1) was fabricated of plywood to a scale of 1:50 to represent the cross-sectional analog of a slender steel deck of a super-long, cable-stayed bridge. The length and width of the section-model were 1600 mm and 510 mm respectively. It consisted of a central open-bottom portion flanked by triangular boxes on the sides. The deck slab of the central portion was supported on diaphragms and cross beams. The bridge deck section-model was adequately stiffened to ensure its own rigidity and it was provided with its full details of railings, kerbs, crash barriers, central verge, etc. At the two ends of the model, elliptical perspex plates were attached to ensure two dimensional flow over and under the model. Fig. 2 shows the section-model in the wind tunnel. The mass (m) and mass moment of inertia (I_α) of the bridge deck section-model were 6.406 kg/m and 0.205 kg-m^2/m respectively.

6.3. Description of the suspension and data acquisition system

The model suspension system (Fig. 2) consisted of 600 mm long horizontal aluminum arms

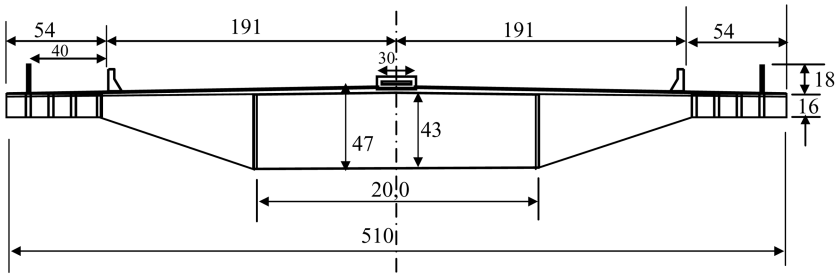

Fig. 1 Bridge deck section-model

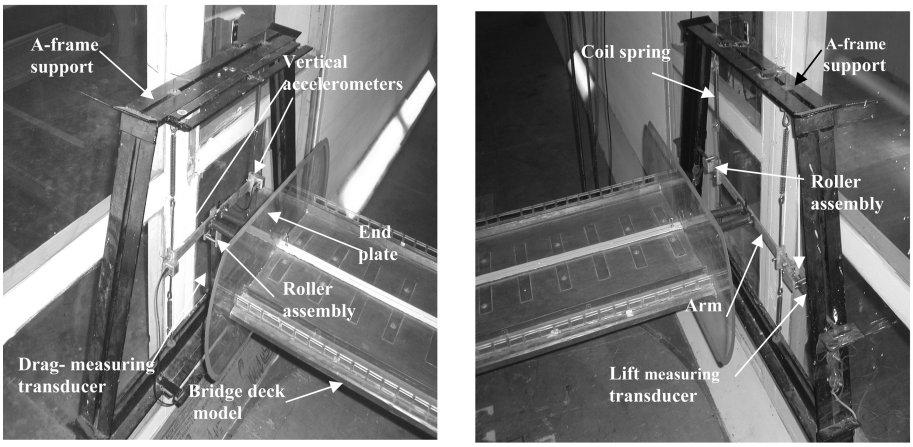

Fig. 2 Suspension and transducer system for wind tunnel test on the bridge deck section-model

connected transversely to brackets of 120 mm length. The bracket with the arm forming a horizontal tee is connected at each end of the model. Four coil-springs (two above and two below the arm), with some degree of pretension, on either side of the models were used to suspend the model by two rigid A-frame supports. The A-frame members consisted of slots at convenient locations. The slots in legs provide extension and seats to the lift measuring transducers. The slots in top and bottom members provide support points to top and bottom suspension springs. The entire assembly fits closely inside the tunnel. This arrangement makes the model free to move along-wind (drag), across-wind (lift) and pitching moment (torsion) directions. Piano wires were also used to arrest motions in a desired degree of freedom while performing free vibration tests.

Phosphor bronze strips were used as cantilever type displacement transducers by pasting a pair of strain gauges at the fixed end of the strip. Three such displacement transducers were used–two for measuring lift motions and one for the drag motion. Two roller assemblies were fixed on both ends of one arm providing free horizontal movement to the two lift-measuring transducers. The spacing between the lift measuring transducers was kept equal to 900 mm. A third drag-measuring transducer along with the roller assembly was fixed on the A-frame brace below the centre of the other arm. The roller assembly consisted of two cylindrical rollers of brass having a gap between them equal to the thickness of transducer strip. Three TML make (spring-mass type) accelerometers

(two for lift and one for drag directions) were also used to obtain the acceleration records of the vertical, horizontal and torsional motions. However, acceleration records have not been used in the present study. All these transducers were properly calibrated. The torsional motion was recorded numerically by the difference of the vertical signals. Let $h_a(t)$ and $h_b(t)$ be the two discrete lift response signals obtained by the transducers at any instant of time and l_{ab} be the horizontal distance between them. Then rotational response at that instant of time is given by:

$$\alpha(t) = \frac{h_a - h_b}{l_{ab}} \tag{29a}$$

and the average vertical response is given as

$$h(t) = \frac{h_a + h_b}{2} \tag{29b}$$

The three sequences of signals h, α and p picked up by strain gauges mounted on phosphor bronze strips were obtained The signals were measured using TML dynamic strain meter (housing signal conditioner, low pass filter and amplifier) and then acquired with the help of a data acquisition (PCL 206 analog to digital conversion) card. The signals were also low-pass filtered electronically at 20 Hz. Care was taken to avoid interference of other electrical and noise signals from the ambience.

6.4. Mechanical properties from no-wind condition

The mechanical (natural) properties such as stiffness ($\boldsymbol{K}^{mech}$) and damping coefficient ($\boldsymbol{C}^{mech}$) of the models were obtained from free vibration records of the model in no-wind condition by giving initial displacements (with the help of weight and pulley arrangement) separately along the three degrees of freedom (h, α and p directions). While imparting free vibration motion along a particular direction, motions along the other two directions were restrained with the help of long piano wires. Several such records were taken and $\boldsymbol{K}^{mech}$, $\boldsymbol{C}^{mech}$ and natural frequencies (ω) of the model corresponding to the three degrees of the freedom were obtained from the average of these parameters obtained from each record. Typical records of free vibration motion of the model are shown in Fig. 3. The values of the natural properties are given in Table 1.

6.5. Stochastic data acquisition and signal processing under wind

The three sequences of responses h, α and p were obtained at wind speeds varying from 3.5 m/s to 15.5 m/s. The signals were amplified with TML dynamic strainmeter (amplifier) and 9000 data points were acquired at a sampling frequency of 240 Hz as raw output data per channel. Samples of raw data time history are presented in Fig. 4. These samples were detrended to remove the offset of

Table 1 The natural properties of the bridge deck section-model

Degree of freedom	ω (rad/s)	K^{mech}	damping ratio (ξ)
h	31.11	9920.279 N/m	0.007
α	44.18	638.847 Nm/rad	0.008
p	22.01	4965.51 N/m	0.021

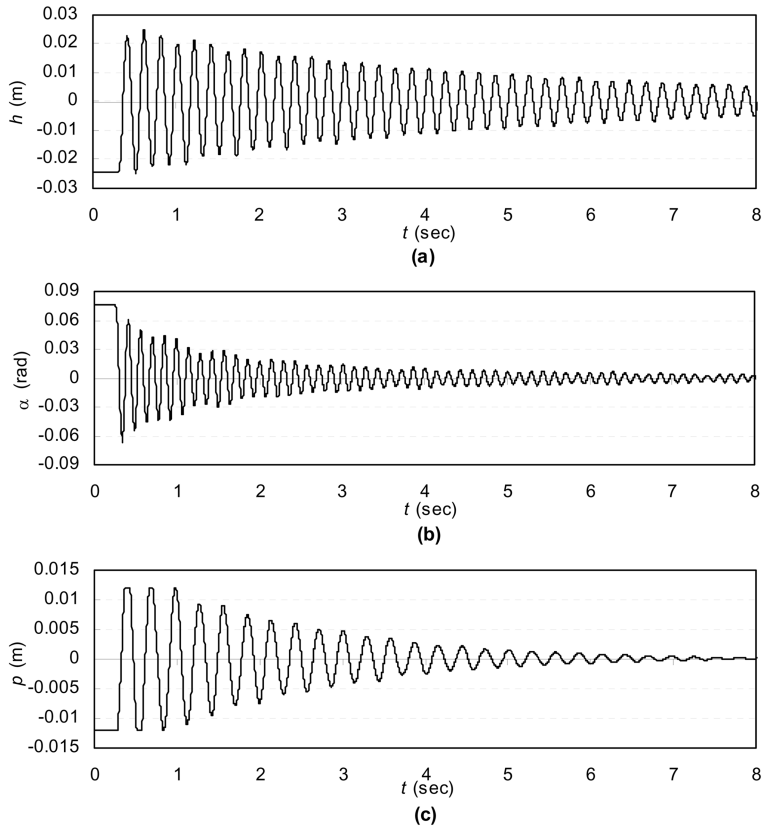

Fig. 3 Free vibration records of bridge deck section-model: (a) Vertical, h (b) Torsional, α (c) Lateral, p

the mean from the baseline. This operation was carried out with the help of MATLAB (1997) detrend command. Before identification the raw output data was lowpass-filtered with an eight-order Chebyshev type I filter with a cutoff frequency of 19.2 Hz. Then the data was resampled at a lower rate of 48 Hz. This whole operation was carried out by the MATLAB decimate command in signal processing toolbox. The cutoff frequency of 19.2 Hz was kept well above the sampling frequency required from the point of view of Nyquist frequency which in turn was well above the largest natural frequency (7.023 Hz) of the sectional model.

6.6. Constitution of Toeplitz matrices and selection of model order

Knowledge of a good model order (system order) is desired for modal analysis. The number of block row i, in Eq. (6) is a user's choice. However, the block rows i and columns of $T_{1|i}$ should be such that $i \geq n_{max}/l$, where n_{max} is the maximum model order. The actual model order in our case is known and is equal to the order of state vector (= 6) and also number of outputs, $l = 3$. The output covariances were determined for lags $k = 1, 2,\ldots, i$. However, higher order of Toeplitz matrix Eq. (6) of $li \times li$ were tried by taking values of block rows, $i = 6, 8,\ldots, 24$. Models of different orders were then obtained by including different number of singular values $\boldsymbol{S}_1$ in the computation of $\boldsymbol{O}_i$ and $\boldsymbol{\Gamma}_i$ from Eqs. (9). Fig. 5 shows typical bar charts depicting the singular values on the ordinate and

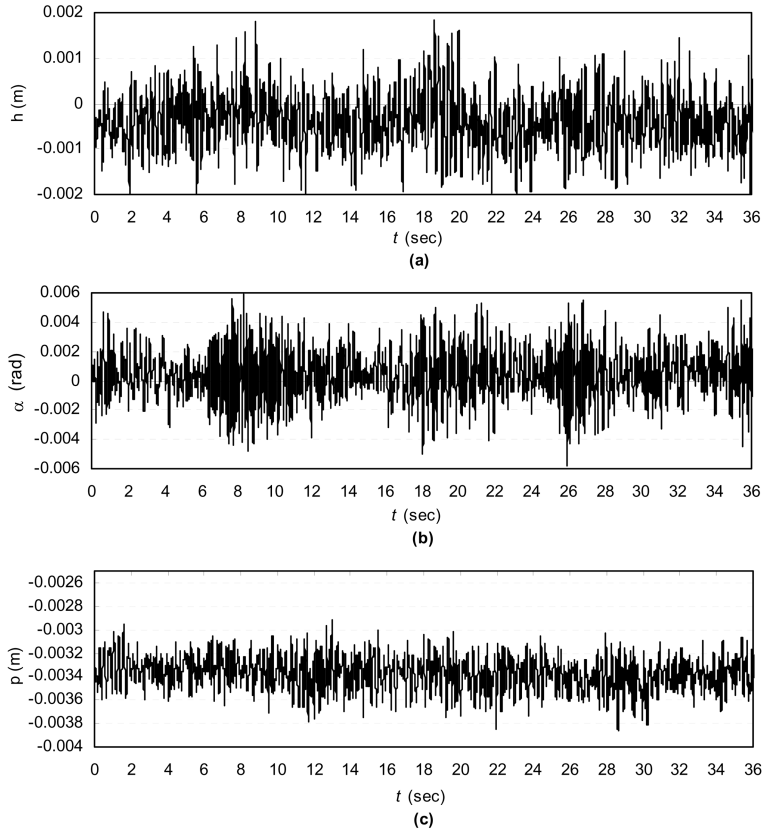

Fig. 4 Displacement record of bridge deck section-model at wind velocity $U = 15.47$ m/s: (a) Vertical, (b) Torsional and (c) Lateral

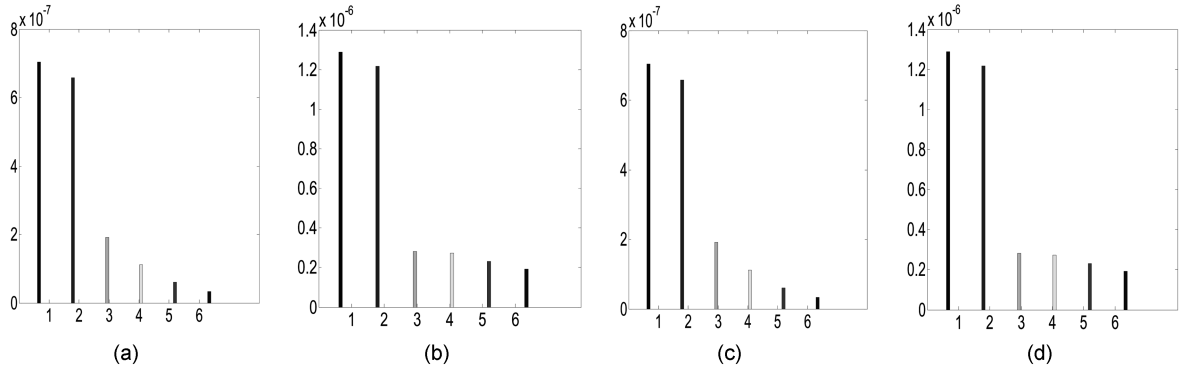

Fig. 5 Typical bar charts showing singular values as ordinates and, number of bars as model order: (a) $U = 6.67$ m/s, $i = 6$; (b) $U = 6.67$ m/s, $i = 16$; (c) $U = 15.47$ m/s , $i = 6$; (d) $U = 15.47$ m/s, $i = 16$

model order on the abscissa for (i) $U = 15.47$ m/s and (ii) $U = 6.67$ m/s each for $i = 6$ and 16. The large differences between singular values of model orders 1 and 6 (Figs. 5(a) and (c)) make the obvious choice of model order equal to 6 which is also the actual model order.

7. Extraction of flutter derivatives

For the implementation of the above technique a computer programme COVSSI was developed in MATLAB. The sequence of steps of implementation is summarized as follows.

For a selected value of number of data, N, a sequence of i values (block rows) varying from 6 to 12 were taken for use in Eq. (5). $T_{1|i}$ and the shifted block Toeplitz matrix $T_{2|i+1}$ were generated based on Eq. (6). Singular value decomposition of $T_{1|i}$ for use in Eq. (8) was done using svd command of MATLAB (1997). Matrix $\boldsymbol{A}$ was realized by selecting a model order equal to 6. MATLAB 'eig' command was used to find mode shape $\boldsymbol{\Phi}$ and continuous time eigen value. Modal frequency ω and damping factor ζ of the system were obtained from Eqs. (13) and (14) respectively. From modal damping and stiffness, physical damping coefficient matrix $\boldsymbol{C}^{eff}$ and stiffness matrix $\boldsymbol{K}^{eff}$ were determined from Eqs. (17) and (19) respectively. These are the submatrices of $\boldsymbol{A}_c$ matrix in Eq. (23). From the already known matrices $\boldsymbol{C}^{mech}$ and $\boldsymbol{K}^{mech}$ and other physical properties of the model the values of 18 flutter derivatives were obtained using Eqs. (24).

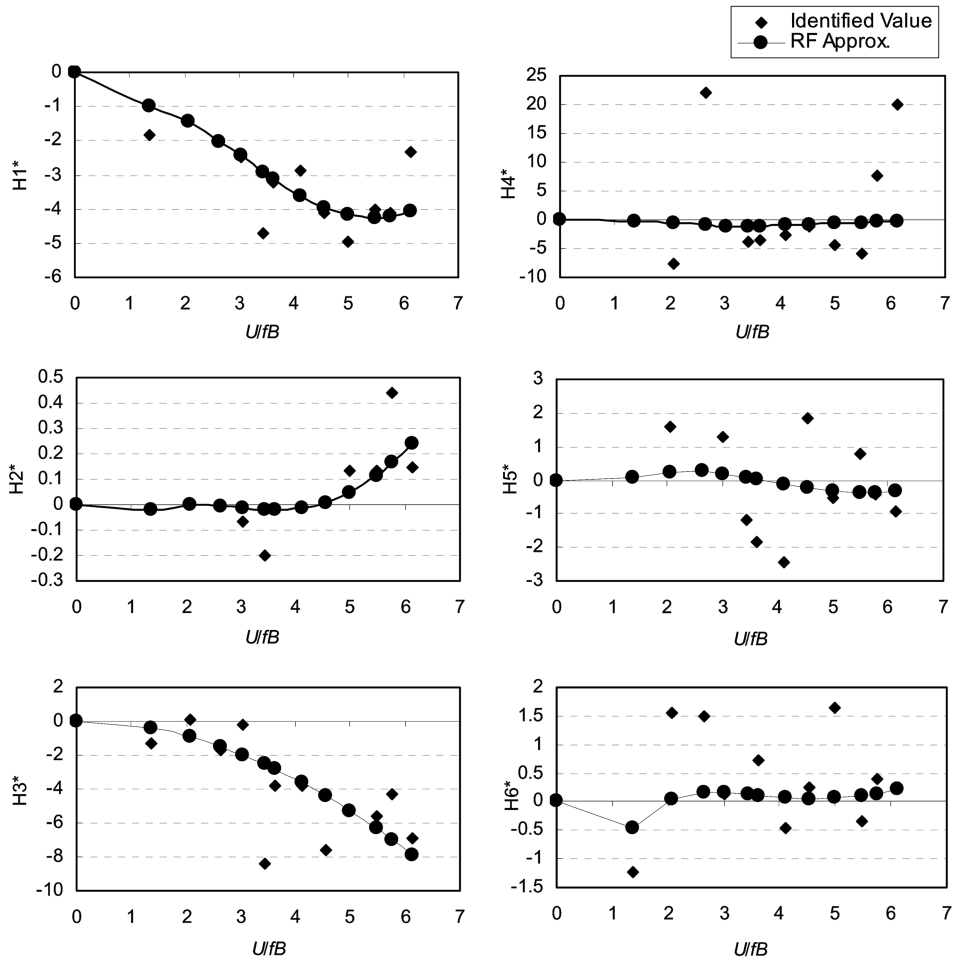

Fig. 6 Vertical flutter derivatives for bridge deck section-model

Values of flutter derivatives at a particular wind speed and for a model order equal to 6 were determined at each value of i. Outliers, if any, were removed and average of flutter derivatives at each wind speed were identified. Vertical (H_i^*), Torsional (A_i^*) and Lateral (P_i^*), ($i = 1,\ldots, 6$) flutter derivatives are presented in Figs. 6, 7 and 8 respectively with respect to reduced velocity, U/fB, where $f = \omega/2\pi$.

The values of flutter derivatives so identified are discretely located. The rational function approximations of the flutter derivatives were obtained as outlined in Section 5. The coefficients of rational function approximation in Eqs. (28) were obtained by developing a computer programme in FORTRAN. The values of the rational function coefficients $\boldsymbol{a}_i^*$ ($i = 1,\ldots, m+3$, $m = 4$) of Eq. (27) have been given in Appendix-I. The approximated curves are shown as continuous curves in Figs. 6, 7 and 8. It is seen that most of the identified flutter derivatives are satisfactorily approximated by the chosen rational function. However, some of the identified flutter derivatives H_5^*, H_6^*, A_1^*, A_2^*, A_3^*, A_5^*, P_1^* are not very well approximated by the rational function taken. The possible reason could be that the same rational terms are used to approximate the pair of flutter derivatives as given in Eq. (28). Another reason could be the fixed values of parameter b in Eq. (28). However, the

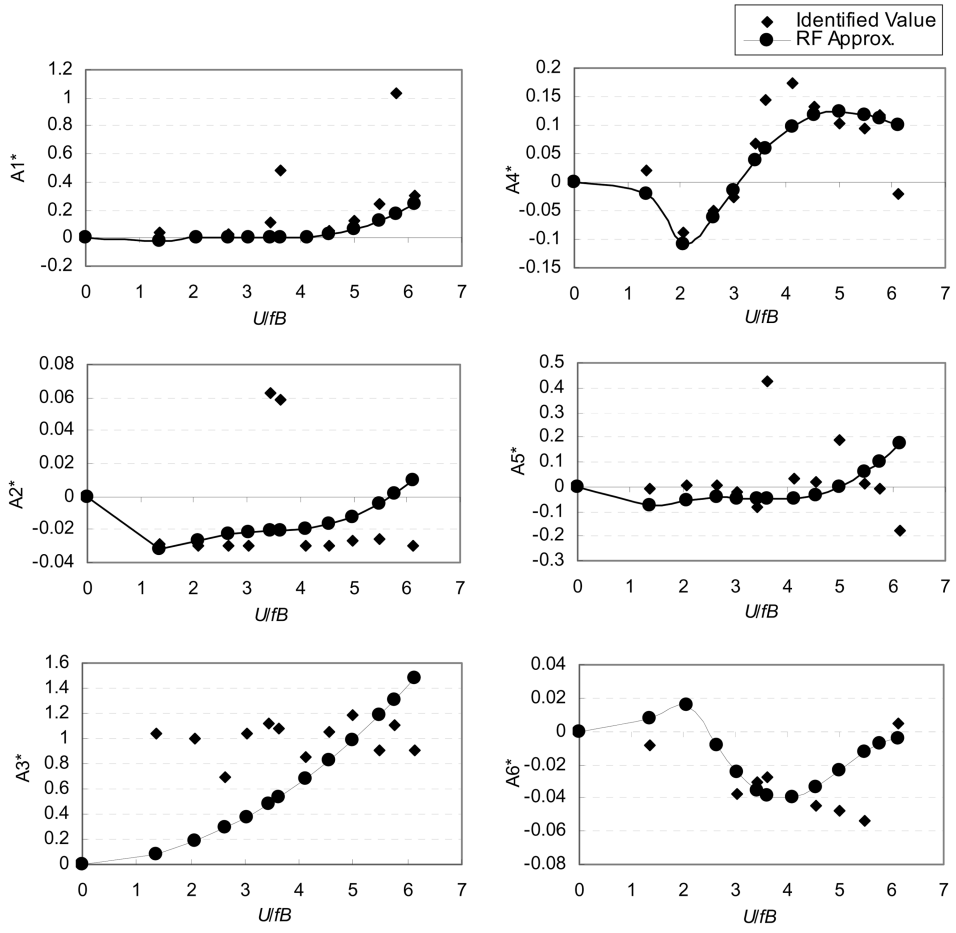

Fig. 7 Torsional flutter derivatives for bridge deck section-model

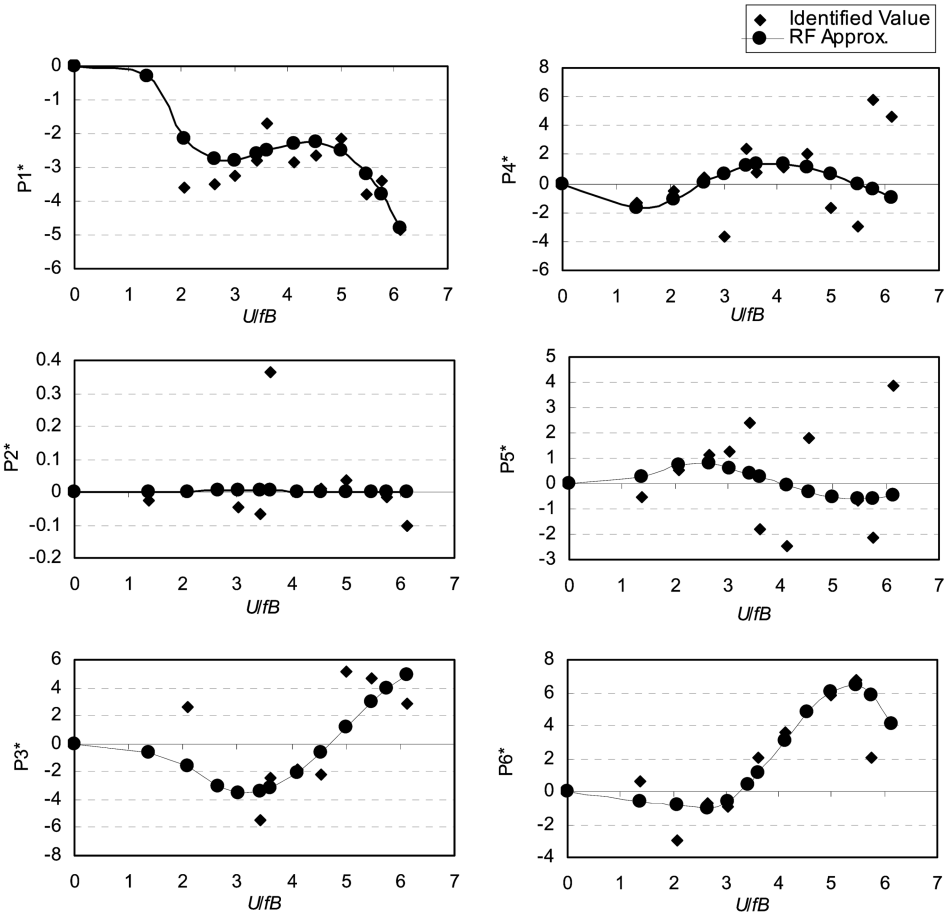

Fig. 8 Lateral flutter derivatives for bridge deck section-model

optimum value of b could also be obtained at the cost of much more involved optimization. The rational function works well. However, a better method of optimization might be a good choice.

8. Discussion and comparison of the flutter derivatives extracted

The authors have not come across any published literature that presents all the 18 flutter derivatives as benchmark for a bridge deck section-model based on wind tunnel experiment. Wherever lateral flutter derivatives have been presented, they have been based on pseudo-steady theory. Therefore, experimental flutter derivatives (Figs. 6-8) of the present bridge deck section-model are compared with their theoretical as well as experimental counterparts available in the literature.

Large scatters are observed in H_4^*, H_5^*, H_6^*, A_2^*, A_3^*, P_4^*, P_5^* in Figs 6-8. In the following, comparison is done for the approximated flutter derivative curves.

The theoretical flutter derivatives for the present bridge deck section-model have been obtained from Theodorsen's and Quasi-steady theory, as presented in Mishra, *et al.* (2005). The general trends of flutter derivatives of the bridge deck section-model H_1^*, H_3^*, H_4^*, H_5^*, A_3^* are well

comparable with their theoretical counterparts. H_2^* does not match with its counterpart. H_6^* and A_6^* are very close to zero, hence acceptable, since their theoretical values are zero. A_1^*, A_2^*, A_4^*, A_5^* are not comparable with the theoretical values. Lateral flutter derivatives also lack resemblance in trend with the Quasi-steady counterparts.

However, a greater degree of resemblance occurs when flutter derivatives of the present bridge deck section-model (Figs. 6-8) are compared with the experimental counterparts determined for real bluff bridge decks such as in Scanlan and Tomko (1971), Simiu and Scanlan (1996), Chowdhury and Sarkar (2003, 2004) and Qin and Gu (2004). Trends and numerical values of H_1^*, H_2^*, H_3^*, H_5^*, H_6^*, A_3^*, A_4^*, A_5^*, A_6^*, P_2^*, P_3^*, P_4^* and P_6^* are comparable with those of Chowdhury and Sarkar (2003, 2004) who have presented all the 18 flutter derivatives based on experiment for the NACA 0020 airfoil. Though, the exact trends of P_1^* and P_5^* are not matching, the downward trend and approximately comparable magnitudes with those of Chowdhury and Sarkar (2004) may make $P_1^*$and P_5^* acceptable.

H_4^*, which has been a difficult parameter, shows large scatter. This scatter has been reported by other authors also such as Jakobsen and Hjorth-Hansen (1993) and Brownjohn and Jakobsen (2001) even in 1-dof case.

Going by the six flutter derivatives H_1^*, H_2^*, H_3^*, A_1^*, A_2^*, A_3^*, presented in Scanlan and Tomko (1971) for different sections, it is seen that the general trends of these flutter derivatives are varying to some extent. With this observation, some greater degree of confidence is added to flutter derivatives extracted in the present study and they can be taken to be practically acceptable.

It is seen that most of the flutter derivatives are following the same pattern as presented either in Scanlan (1971), or in Qin and Gu (2004). The scatter in the identified values of flutter derivatives may be attributed to the stochastic identification method itself. The presence of railings, crash barriers and the open soffit of the bridge deck may be considered as other factors contributing to the scatter in the identified values. Good match of trends in the case of H_1^*, H_2^*, H_3^*, H_5^*, H_6^*, A_3^*, A_4^*, A_5^*, A_6^*, P_2^*, P_3^*, P_4^* and P_6^* are found between this identification and that identified by iterative least square method used by Chowdhury and Sarkar (2003). However, very few published reported values are there about the simultaneous identification of the maximum number of flutter derivatives.

9. Conclusions

All the eighteen flutter derivatives have been identified by the covariance driven stochastic subspace identification (COV-SSI) method using the output-only measurement of displacements along the lift, drag and torsional degrees of freedom of a bridge deck section-model. The discretely identified values of flutter derivatives have been approximated by rational functions to obtain these as continuous functions of reduced frequency. The efficiency and simplicity of the COV-SSI method lies in output-only measurements and its noniterative nature of computations. The method uses only output measurements and therefore instrumentation and extra efforts of input measurements are eliminated. Some flutter derivatives such as H_4^*, H_5^*, H_6^*, A_2^*, A_3^*, P_4^* and P_5^* do not show clear trends because of the scatter in their identified values. The scatter in the values may be attributed to the stochastic method itself which can be minimized by adopting better signal processing techniques. The presence of railings, crash barriers, central verge and the open soffit of the bridge deck may be the other factors contributing to the scatter in the identified values. However, very few reported values based on test results are available for the full set of 18 flutter derivatives and therefore more research in this area is needed. The overall performance of the COV-SSI method has good potential in flutter derivative extraction.

Appendix-I

Values of rational function coefficients for the experimentally determined flutter derivatives

$$a_1^* = \begin{bmatrix} -11.4383 & -2.0204 & -10.075 \\ -2.3828 & 26.2961 & -0.7626 \\ 1.4571 & -1.7477 & 1.2954 \end{bmatrix}; \quad a_2^* = \begin{bmatrix} 0.0107 & 0.01020 & 0.01005 \\ 0.0041 & 0.0084 & 0.00997 \\ -1.94703 & 0.4564 & 0.01005 \end{bmatrix}$$

$$a_3^* = \begin{bmatrix} -0.0002 & -0.0010 & -0.00001 \\ -0.0010 & -0.0010 & -0.0010 \\ -0.0001 & -0.0001 & -0.0010 \end{bmatrix}; \quad a_4^* = \begin{bmatrix} 22.3933 & 7.5063 & 3.1079 \\ 18.5762 & -58.9053 & 0.0669 \\ -3.16531 & 3.0676 & 0.4048 \end{bmatrix}$$

$$a_5^* = \begin{bmatrix} -48.7781 & -28.6746 & -5.6679 \\ -69.0004 & 186.5316 & -0.3199 \\ 15.2333 & -6.8384 & -1.0267 \end{bmatrix}; \quad a_6^* = \begin{bmatrix} 203.1276 & 121.1408 & 22.6527 \\ 274.2314 & -882.7018 & 2.1382 \\ -137.7586 & 43.4001 & 9.1791 \end{bmatrix}$$

$$a_7^* = \begin{bmatrix} -232.0812 & -108.2237 & -21.8808 \\ -235.5101 & 809.9971 & -2.2683 \\ 171.1410 & 50.6278 & -10.7985 \end{bmatrix}$$

References

Akaike, H. (1974), "Stochastic theory of minimal realization", *IEEE Tran. Auto. Contr.*, **19**, 667-674.

Bevington, P.R. (1969), *Data Reduction and Error Analysis for the Physical Sciences*, Mac-Graw Hill, New York.

Boonyapinyo, V., Miyata, T. and Yamada, H. (1999), "Advanced aerodynamic analysis of suspension bridges by state space approach", *J. Str. Eng.*, ASCE, **125**(12), 1357-1366.

Brownjohn, J.M.W. and Jakobsen, J.B. (2001), "Strategies for aeroelastic parameter identification from bridge deck free vibration data", *J. Wind Eng. Ind. Aerodyn.*, **89**, 1113-1136.

Bucher, C.G. and Lin, Y.K. (1988), "Stochastic stability of bridges considering coupled modes", *J. Eng. Mech.*, ASCE, **114**(12), 2055-2071.

Chen, X., Matsumoto, M. and Kareem, A. (2000a), "Time domain flutter and buffeting response analysis of bridges", *J. Eng. Mech.*, ASCE, **126**(1), 7-16.

Chen, X., Matsumoto, M. and Kareem, A., (2000b), "Aerodynamic coupling effects on the flutter and buffeting of bridges", *J. Eng. Mech.*, ASCE, **126**(1), 17-26.

Chen, A., He, X. and Xiang, H. (2002), "Identification of 18 flutter derivatives of bridge decks", *J. Wind Eng. Ind. Aerodyn.*, **90**, 2007-2022.

Chen, X. and Kareem, A. (2002), "Advances in modeling of aerodynamic forces on bridge decks", *J. Eng. Mech.*, ASCE, **128**(11), 1193-1205.

Chowdhury, A.G. and Sarkar, P.P. (2003), "A new technique for identification of eighteen flutter derivatives using a three-degree-of-freedom sectional model", *Eng. Str.*, **25**, 1763-1772.

Chowdhury, A.G. and Sarkar, P.P. (2004), "Identification of flutter derivatives of an airfoil and bridge deck", *Wind and Str.*, **7**(3), 187-02.

Craig, R.R. Jr. (1981), *Structural Dynamics*, John Wiley, New York.

Gu, M., Zhang, R. and Xiang, H. (2000), "Identification of flutter derivatives of bridge decks", *J. Wind. Eng. Ind. Aerodyn.*, **84**, 151-162.

Guyan, R.J. (1965), "Reduction of stiffness and mass matrices", *AIAA J*., **3**(2), 380.
Ho, B.L. and Kalman, R.E. (1966), "Effective construction of linear state-variable models from input/output data", *Regelungstechnik*, **14**, 545-548.
Jakobsen, J. B. and Hijorth-Hansen, E. (1993), "Determination of the aerodynamic derivative by system identification method", *Wind Engineering: 1st AWE European and African Regional Conference*, Cook. N. J. (ed.), 367-377, Thomas Telford.
Juang, J.N and Pappa, R.S. (1985), "An eigensystem realization algorithm for modal parameter identification and model reduction", *J. Guid. Contr. Dyn*., **5**, 620-627.
Juang, J.N. (1994), *Applied System Identification*, Prentice-Hall, Englewood Cliffs, NJ.
Ljung, L. (1987), *System Identification Theory for the User*, 1st ed., Prentice Hall Inc. Englewood Cliffs, NJ, USA.
MATLAB (1997), *Signal Processing Toolbox for Use with Matlab*, User's Guide Version 4, The Mathworks Inc, Nattick, MA, USA [http://www.mathworks.com].
Mishra, S.S. (2005), "Effect of wind drag on flutter of long-span cable-stayed bridge decks", Ph. D. thesis, Indian Institute of Technology Roorkee, India.
Overschee, P.V. and Moor, B.D. (1993), "Subspace algorithm for the stochastic identification problem", *Automatica*, **29**(3), 649-660.
Peeters, B. and Roeck, G.D. (1999), "Reference-based stochastic subspace identification for output-only modal analysis", *Mech. Sys. Sig. Proc*., **13**(6), 855-78.
Peeters, B. (2000), "System identification and damage detection in civil engineering", Ph. D. Thesis, KU Leuven, Belgium.
Press, W.H., Teukolsky, S.A. and Vellerling, W.T. and Flannery, BP. (1992), *Numerical Recipes in FORTRAN*, 2nd ed., Cambridge Univ. Press.
Qin, X.R. and Gu, M. (2004), "Determination of flutter derivatives by stochastic subspace identification technique", *Wind Struct*., **7**(3), 173-186.
Roger, K.L. (1977), "Airplane Math Modeling Methods for Active Control Design", *Str. Aspects of Active Control*, Agard -CP-228, 4-1-4-11.
Sarkar, P.P., Jones, N.P. and Scanlan, R.H. (1994), "Identification of aeroelastic parameters of flexible bridges", *J. Eng. Mech*., ASCE, **120**(8), 1718-1742.
Scanlan, R.H. and Tomoko, J.J. (1971), "Airfoil and bridge deck flutter derivatives", *J. Eng. Mech. Div*., ASCE, **97**(6), 1717-1733.
Scanlan, R.H. (1978), "The action of flexible bridges under wind. I: flutter theory", *J. Sound and Vib*., **60**(2), 187-199.
Simiu, E. and Scanlan, R.H. (1996), *Wind Effects on Structures*, 3rd Ed., John Wiley & Sons, Inc. New York.
Singh, L., Jones, N.P., Scanlan, R.H. and Lorendeaux, O. (1995), "Simultaneous identification of 3-D of aeroelastic parameters", *Proceedings of. 9th Int. Conf. on Wind Eng*., New Delhi, India, 872-81.
Zhu, L.D., Xu, Y.L., Zhang, F. and Xiang, H.F. (2002), "Tsing Ma bridge deck under skew winds. Part II: Flutter derivatives", *J. Wind Eng. Ind. Aerodyn*., **90**, 807-837.
Zeiger, H.P. and McEwen, A.J. (1974), "Approximate linear realization of given dimension via Ho's algorithm", *IEEE Trans. Auto. Contr*., **AC-19**(2), 153.

CC